Electronic Supplementary Information for

The Role of Chemisorbed Hydroxyl Species in Alkaline Electrocatalysis of Glycerol on Gold

X. Shi, D. E. Simpson and D. Roy*

Department of Physics, Clarkson University, Potsdam, New York 13699-5820, USA
**To whom correspondence should be addressed. E-mail: samoy@clarkson.edu*

1. Supplementary details of experimental considerations and procedures

The OH^- content of the experimental supporting electrolyte was comparable to those frequently used in full DGFCs,[S1, 2] but about an order of magnitude lower than those often employed for laboratory scale half-cell studies of such systems. The relatively strong OH^- concentration was chosen here to ensure an adequate supply of surface bound OH^- at the Au anodes, as well as to minimize the effects of ohmic drop at the electrode interface.[S3] The glycerol (Gly) concentrations were set at 1.0 M (comparable to those used in full DGFCs) and 0.03 M for the stationary and the rotating electrodes, respectively. These somewhat moderate Gly concentrations were employed to bring out the mass transport controlled features of Gly oxidation. The Gly concentrations were optimized according to the hydrodynamic conditions of the cell (stationary or rotating electrode) in a separate set of experiments by carefully monitoring the peaks and plateaus of the oxidation currents.

The electrolytes were not de-aerated for electrochemical measurements. The solution resistances (R_s) as well as the double layer capacitances (C_{dl}) for the electrolytes were measured by using electrochemical impedance spectroscopy (EIS).[S4] This was necessary to incorporate ohmic corrections in the analysis of current peaks, and to subtract baseline double layer currents in the integration of voltammograms to determine faradaic reaction charges.[5] R_s was voltage independent, with a value of 2.7 Ω cm^2 for the solutions used. The values of C_{dl} varied between 20 and 60 μF cm^{-2} depending on the applied voltage and the solution composition. The potential dependent double layer currents, vC_{dl}, were evaluated to extract the faradaic currents from the experimental voltammograms (v denotes the voltage scan speed of CV).

The voltage ranges of the limiting current plateaus obtained in the RDE measurements were simultaneously dictated by the values of v and ω. Following previously published reports for similar electro-catalytic systems, the voltage scan speeds for RDE-CV were chosen within the 20-50 mV s^{-1} range.[S6, 7] The corresponding disc rotation speeds necessary to maintain adequate limiting current plateaus were typically maintained between 80 and 900 rpm. This selected range of ω was checked against the following standard criterion for validating RDE measurements: $10 < [(\omega r^2)/\nu_e] < 2\times10^5$, for aqueous electrolytes at room temperature.[S3] ν_e is the kinematic viscosity of the electrolyte (0.01 cm^2 s^{-1} at room temperature) and r is the radius of the RDE

(0.317 cm). With these values, the quantity $[(\omega r^2)/\nu_e]$ varied between 84 and 947 corresponding to varying ω from 80 to 900 rpm, respectively. Thus, all the RDE experiments reported here were performed under adequate conditions necessary for such measurements.

The electrochemical measurements were strategically centered on quantitative utilization of the CV technique. Since structurally solid electrodes (as opposed to particle-based composites) were used in this work, additional measurements[S8, 9] were not necessary to check the catalyst's stability. The CV experiments used a Pt counter electrode and an SCE reference in a cell configuration similar to those used by previous authors to study similar systems.[S10, 11] When immersed in acidic electrolytes, Pt counter electrodes often tend to slightly dissolve, which can result in low level deposition of Pt on the working electrode.[S12, 13] According to the Pourbaix diagram of Pt, however, such a process should not be supported in the strong alkaline medium used here.[S14] Nevertheless, as a preventive measure, the Pt electrode employed for this work was encased in a glass cylinder that opened to the solution through a permeable flat end. Before each experiment the polycrystalline electrodes were polished on a polisher (a 3" diameter rotating table, covered with Buehler Microcloth™), using aqueous pastes of 1.0, 0.3 and 0.05 μm alumina particles in successive steps.

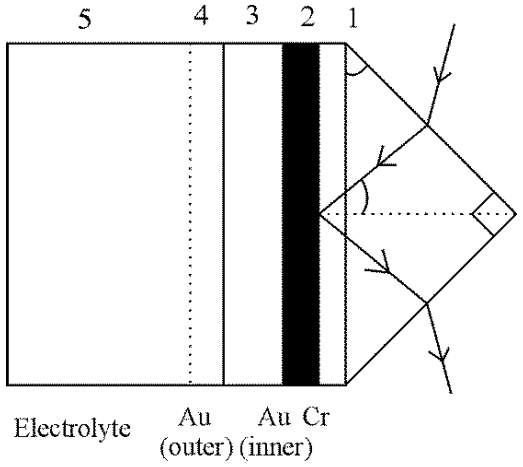

Figure S1. Setup used for SPR and CV experiments involving the Au film electrode. The path of the probe light is shown with the arrows.

The optical configuration used for the angle-resolved surface plasmon resonance (SPR) measurements is schematically shown in Fig. S1. The different layers of the multi-layer system are labeled 1-5. Layer 1 denotes the SF 10 light-coupling 90 degree prism, optically attached to the SF 10 substrate of the Au sample by using a refractive index matching fluid. Layers 2 and 3 are the Cr binding film and the inner region of the Au film, respectively. Layer 4 is the outer region of the Au film, which is optically affected by interactions of the electrolyte (only counted as a separate layer in the multi-phase model used to determine the individual layer thicknesses). Layer 5 is the electrolyte, and the interface of layers 4 and 5 represents the active region of electrochemical reactions.

The thicknesses of the Cr and Au layers of the film electrode were determined by fitting a separate set of SPR data (collected for calibration) to a five-phase model by using known optical parameters of the multi-layer system;[S15] these calculations were performed with MATLAB™ codes developed by the authors' group.[S16] Prior to each experiment, the Au film electrode was cleaned as described previously.[S15, 17] Both CV and SPR measurements for the Au film were performed by using the film electrode in a Teflon cell described elsewhere.[S16, 18, 19]

2. Supplementary results and notes

2.1. Tafel analysis of RDE CV data

The intercept of the Koutecký-Levich plots used here to study Gly oxidation is related to the effective exchange current density (i_0) of the net oxidation reaction. However, the value of this intercept is specific to the choices of η,[S6] and represents composite results of multiple ω values.

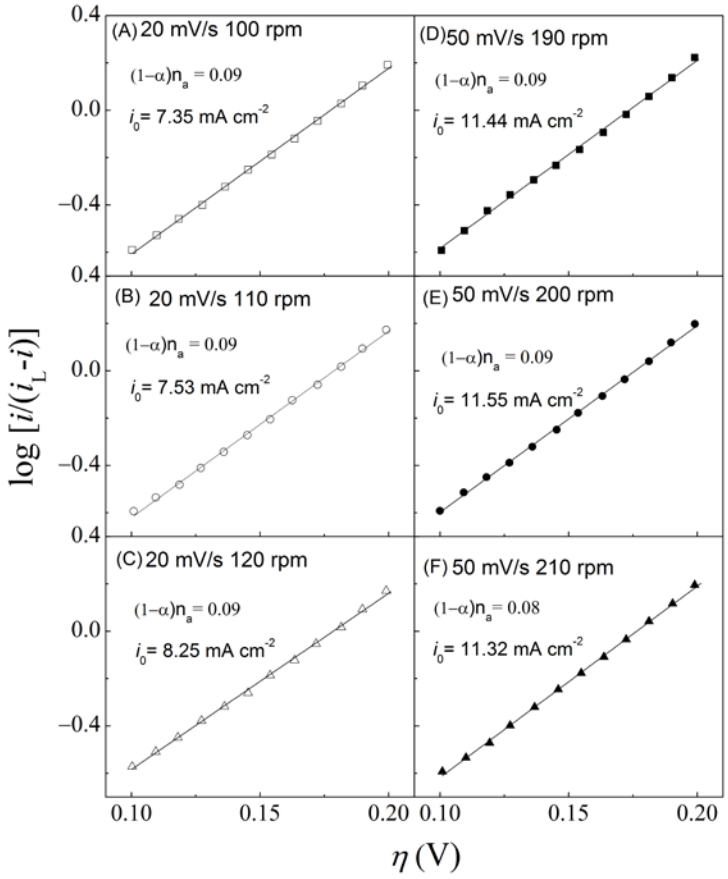

Figure S2. Tafel plots for the Au polycrystalline RDE, recorded at different rates of voltage sweep (V s^{-1}) at different rates of disc rotation (rpm). The linear fits to the data points provide the values of $(1-\alpha)n_a$ and i_0 in each panel.

Since the anodic potential for the onset of Gly oxidation varies with changes of ω in the present system, any incorporation of a single value of η for a full Koutecký-Levich plot can introduce a sizeable uncertainty in the calculation of i_0 taken from the intercept of such a plot. Moreover, depending on the experimental system, the accuracy of such calculations based on the Koutecký-Levich intercept can be voltage dependent.[S20] Therefore, Levich and Koutecký-Levich analyses were not attempted in this work to evaluate i_0; instead Tafel analysis was used to determine i_0.

Fig. 10 of the main article shows a composite Tafel plot, combining the 20 and 50 mV s^{-1} CV data for different angular speeds of RDE rotation. These data are separately shown here in Fig. S2 for the individual scan speeds of CV and the individual rotation rates of the RDE. The left and the right columns in Fig. S2 correspond to voltage scan rates of 20 and 50 mV s^{-1}, respectively. The symbols are data points and the solid traces are linear fits to the data. The values of i_0 and those of the RDS parameter $n_a(1-\alpha)$ obtained from these fits are indicated in the Figure.

For each scan rate of CV used in the RDE experiments, three different electrode rotation speeds were applied. The values of $n_a(1-\alpha)$ obtained for the different cases were quite comparable. The exchange currents determined in Fig. S2 vary between 7 and 11 mA cm^{-2}, which are values comparable to those previously reported for similar electrocatalytic reactions on efficient catalyst substrates.[S21] The electron-counts monitored under controlled variations of forced convection in the RDE measurements illustrate the role of mass transport in the IHO promoted oxidation kinetics of Gly.

The exchange current exhibits a slightly increasing trend with increasing speeds of disc rotation as the convective transport of reactants is correspondingly facilitated. The composite plot in Fig. 10 of the article yielded $n_a(1-\alpha) = 0.09$ and $i_0 = 9.59$ mA cm^{-2}. As expected in terms of the "averaged" nature of the linear fit used there, these values are comparable to the parameters shown above in the separate panels of Fig. S2.

2.2. Implications of the effective electron counts (n values) obtained from scan rate controlled CV, Levich plots and Koutecký–Levich plots

The present work uses a relatively simple method of determining the surface reaction mechanisms of Gly by constructing a "voltammetric registry" of faradaically activated electron-counts. The results have been confirmed by comparing the oxidation products implied by these electron counts with those previously reported by using various other analytical techniques. The values of *n* found from Figs. 3 and 4 of the main article represent *effective* values of this parameter resulting from multiple criteria of averaging the *Koutecký* electron-yields, and these criteria are implicit in the associated measurements employed. The first criterion of this averaging effect comes from the simultaneous presence of reactions (8) and (11). Following the approach of previous authors,[S22, 23] we have used here the bulk concentration of Gly as the value of c_b to calculate *n* from eqns (2) and (3) of the main report. The *n* value resulting from this

approach represents a concentration-weighted average of the contributions of Gly and Gly^- [according to eqns (8) and (11), respectively] at the given solution pH. Nevertheless, since both Gly and Gly^- oxidize to glyceraldehyde via two-electron pathways, the considerations for this averaging are relatively less critical in the present case.

The possibility of site-specific distribution in the values of *n* introduces the second inherent averaging feature in the calculation of *n*.[S24] Moreover, since the oxidation products of Gly (or Gly^-) are generated in a sequential process, the resulting *n* can be voltage dependent in the course of a progressing anodic scan, with the higher values of *n* emerging mostly from the upper region of the scan.[25] Thus the net result for *n* obtained from Fig. 3C/4C likely contains an average signature of the *n*(*E*) values emerging from the full scan range of CV used here.

References

S1. A. P. Nascimento and J. J. Linares, *J. Braz. Chem. Soc.*, 2014, 25, 509-516.
S2. S. R. Ragsdale and C. B. Ashfield, *ECS Trans.*, 2008, 16, 1847-1854.
S3. L. R. F. Allen J. Bard, *Electrochemical Methods Fundamentals and Applications*, John Wiley & Sons, New York, 2001.
S4. J. E. Garland, C. M. Pettit and D. Roy, *Electrochim. Acta*, 2004, 49, 2623-2635.
S5. S. B. Emery, J. L. Hubbley and D. Roy, *Electrochim. Acta*, 2005, 50, 5659-5672.
S6. D. A. Finkelstein, N. D. Mota, J. L. Cohen and H. D. Abruña, *J. Phys. Chem. C*, 2009, 113, 19700-19712.
S7. G. Hou and J. Prakash, *ECS Trans.*, 2006, 1, 27-33.
S8. A. N. Geraldes, D. F. Silva, J. C. M. Silva, R. F. B. Souza, E. V. Spinacé, A. O. Neto, M. Linardi and M. C. Santos, *J. Braz. Chem. Society*, 2014, 25, 831-840.
S9. Y. Shen, Z. Zhang, K. Xiao and J. Xi, *Phys. Chem. Chem. Phys.*, 2014, 16, 21609-21614.
S10. J. S. Gordon and D. C. Johnson, *J. Electroanal. Chem.*, 1994, 365, 267-274.
S11. K. Juodkazis, J. Juodkazytė, T. Juodienė and A. Lukinskas, *J. Electroanal. Chem.*, 1998, 441, 19-24.
S12. A. Hamelin, *J. Electroanal. Chem.*, 1996, 407, 1-11.
S13. J. Solla-Gullón, A. Aldaz and J. Clavilier, *Electrochim. Acta*, 2013, 87, 669-675.
S14. J. V. M. M. J. N. Pourbaix, N. de Zoubov, *Platinum Metals Rev.*, 1959, 3, 47-53.
S15. C. M. Sulyma, C. M. Pettit, J. E. Garland and D. Roy, *Surf. Interface Anal.*, 2012, 44, 801-810.
S16. K. A. Assiongbon and D. Roy, *Surf. Sci.*, 2005, 594, 99-119.
S17. J. E. Garland, K. A. Assiongbon, C. M. Pettit and D. Roy, *Anal. Chim. Acta*, 2003, 475, 47-58.
S18. C. M. Pettit and D. Roy, *Analyst*, 2007, 132, 524-535.
S19. C. M. Pettit, K. A. Assiongbon, J. E. Garland and D. Roy, *Sens. Actuator B*, 2003, 96, 105-113.
S20. F. J. Vidal-Iglesias, J. Solla-Gullón, V. Montiel and A. Aldaz, *Electrochem. Commun.*, 2012, 15, 42-45.

S21. S. B. C. Coutanceau and M. Simões, in: Catalyste for Alcohol Fuelled Direct Oxidation Fuel Cells, Eds. X.X Liang and T. S. Zhao, Royal Society of Chemistry, Cambridge, 2012, vol. 6, ch.
S22. D. M. F. Santos and C. A. C. Sequeira, *Electrochim. Acta*, 2010, 55, 6775-6781.
S23. J. Hou, M. W. Ellis and R. B. Moore, *Electrochem. and Solid-State Lett.*, 2012, 15, B39-B43.
S24. M. D. Levi, N. V. Fedorovich and B. B. Damaskin, *Canadian J. Chem.*, 1981, 59, 2019-2025.
S25. G. Hou, J. Parrondo, V. Ramani and J. Prakash, *J. Electrochem. Soc.*, 2014, 161, F252-F258.